

## Research Article

## Role of Constitutive Modeling on the Analysis of Shear Localization in Semi-Solid Deformation

M.H. Sheikh-Ansari and M. Aghaie-Khafri\*

Faculty of Materials Science and Engineering, K.N. Toosi University of Technology, Postal Code: 1999143344, Tehran, Iran

## ARTICLE INFO

## Article history:

Received 2 February 2025

Reviewed 1 March 2025

Revised 13 March 2025

Accepted 3 April 2025

## Keywords:

Shear localization  
Semi-solid deformation  
Dilatancy  
Perturbation analysis  
Constitutive model

## Please cite this article as:

Sheikh-Ansari, M. H., & Aghaie-Khafri, M. (2025). Role of constitutive modeling on the analysis of shear localization in semi-solid deformation. *Iranian Journal of Materials Forming*, 12(2), 4-14.  
<https://doi.org/10.22099/IJMF.2025.52371.1325>

## ABSTRACT

This study presents an analytical framework to investigate the role of constitutive modeling in evaluating the instability of semi-solid deformation. Two constitutive models' distinct conceptual foundations are considered. The first model characterizes mushy-state deformation as an interpolation between the behaviors of porous and cohesionless granular materials. The second model adopts the Norton-Hoff viscosity law to describe the rheology of semi-solid alloys. The evolution of small perturbations is examined in relation to key constitutive parameters. Both models predict that increased rate sensitivity mitigates the likelihood of shear localization, whereas higher strain rates tend to promote it. However, the models diverge in their predictions regarding the effect of cohesion. The viscosity-based model exhibits stronger agreement with recent X-ray tomography studies and experimental data from tests on 7075 aluminum alloy, indicating its superior capability in capturing semi-solid rheological behavior. Furthermore, this model predicts the existence of a critical strain rate, above which semi-solid deformation becomes unstable for a given cohesion degree. In contrast, the Zavaliangos model suggests that the tendency for localization increases with cohesion, an outcome that contradicts experimental findings. This discrepancy is substantiated through parameterization and quantitative analysis.

© Shiraz University, Shiraz, Iran, 2025

| Nomenclature                 |   | $\sigma_h$                      | The hydrostatic part of the stress tensor  |
|------------------------------|---|---------------------------------|--|
| $\dot{\epsilon}_e$           | Deviatoric part of the plastic strain rate  | $p_L$                           | The liquid pressure  |
| $\sigma_e$                   | Von-Mises stress  | $(\sigma_e)_{viscous}$          | Effective stress   |
| $\Xi$                        | The viscoplastic potential  | $\dot{\epsilon}_{eff}$          | Effective strain rate  |
| $n$                          | Power law index   | $\eta(c, \dot{\epsilon}_{eff})$ | The viscosity as a function of the cohesion degree and the effective strain rate |
| $A_0, A_c$                   | Two functions of the solid fraction which defined according to the relations proposed by Zavaliangos (1998) | $\mathbf{b}$                    | Internal forces  |
| $\phi'$                      | The angle of the critical state line in the Cam-clay model  | $\mathbf{u}$                    | Displacement   |
| $m$                          | Rate sensitivity parameter  | $\mathbf{M}$                    | The fluid flux   |
| $\mu$                        | Frictional coefficient  | $\chi$                          | Permeability   |
| $c$                          | Cohesion degree   | $\zeta$                         | Dilatational strain  |
| $\dot{\epsilon}_0, \sigma_0$ | Material parameters   | $\beta$                         | Dilatancy ratio  |

\* Corresponding author

E-mail address: [maghaei@kntu.ac.ir](mailto:maghaei@kntu.ac.ir) (M. Aghaie-Khafri)<https://doi.org/10.22099/IJMF.2025.52371.1325>

## 1. Introduction

Semi-solid deformation is an advanced manufacturing technique that enables the production of near-net-shaped parts with enhanced mechanical properties. This process improves production efficiency by eliminating the need for complex molds and simplifying operations, while preserving essential material characteristics such as electrical and thermal conductivity. Compared to conventional solid-state metal forming, semi-solid processing requires lower forming pressures and shorter processing cycles, thereby facilitating the production of fine-grained alloys with superior mechanical performance [1-7].

The unique characteristics of semi-solid deformation arise from the thixotropic behavior of alloys in the mushy state, where viscosity decreases under applied shear stress. This property is crucial for shaping and forming materials during manufacturing [8-10]. Thixotropy is influenced by key factors such as temperature, microstructure, and shear rate. Higher solid fractions enhance viscoelasticity, meaning that thixotropic alloys exhibit both flow and elastic behavior under stress [11-14].

The initial microstructure, particularly the size, shape, and distribution of solid particles, has a significant impact on thixotropic strength. Deagglomeration promotes shear thinning, and the resulting flow softening can contribute to shear localization [15, 16]. Tzimas and Zavaliangos [17] observed that when the liquid content is low, compression loading induces high non-uniformity, leading to strain instability. They proposed that shear localization results from solid bond decohesion and dilatancy, referring to the local expansion of the solid skeleton.

Semi-solid deformation involves complex interactions between solid and liquid phases, which significantly influence material properties and processing outcomes. Studies on 7075 aluminum alloys have shown that inter-granular deformation compensates for liquid shrinkage, enhancing component integrity, while intra-granular deformation modifies grain morphology and induces sub-grain boundaries [18, 19].

Simulations using multi-phase-field lattice, Boltzmann models and discrete element methods have revealed granular behaviors such as dilatancy and shear localization, which depend on grain morphology and solid fraction [20-22]. In-situ X-ray tomography experiments have further demonstrated that grain refinement occurs through liquation-assisted transgranular cracking [23].

Morita et al. [24] using in-situ observations, studied the deformation process of semi-solid steel and found that solid grains dynamically rearrange during deformation, forming regions with reduced solid fractions. Nagira et al. [25] observed that force transfer occurs through grain contacts aligned with the shear loading direction, with shear strain rates concentrating in localized bands.

Given the complexity of semi-solid deformation, various constitutive models have been developed based on different assumptions [26]. Some models treat semi-solid materials as porous media, where liquid-phase flow follows Darcy's law [27-30]. Others incorporate internal structural parameters to analytically describe rheology [31-34]. Additionally, phenomenological viscoplastic models derived from solid-state formulations [35, 36], and micromechanics-based homogenization models [37-39] have been proposed.

For rate-independent materials, instability is often analyzed as a deviation from homogeneous deformation, mathematically characterized by the loss of ellipticity in the equilibrium velocity equations [40-45]. However, Lemonds and Needleman [46] demonstrated that ellipticity loss does not apply to rate-dependent materials. In such cases, an alternative approach involves introducing infinitesimal perturbations to model parameters and analyzing their growth over time [47-52].

The intricate nature of semi-solid microstructures presents significant challenges in the development of accurate constitutive models. Semi-solid materials exhibit both solid-like and liquid-like behaviors, resulting in complex deformation mechanisms that require specialized modeling approaches. Key factors influencing constitutive models for semi-solid materials

include their multi-phase composition, strain rate sensitivity, temperature dependence, particle interactions, and rheological complexity. Since localization in such granular media is affected by each of these factors, the selection of constitutive model plays a crucial role in the accuracy of localization analysis. To the best of the authors' knowledge, the influence of constitutive modeling on localization analysis in semi-solid deformation has not been previously addressed. Given the rate-dependent nature of semi-solid deformation, this study employs linear perturbation analysis to derive shear localization conditions for two different constitutive models.

## 2. Constitutive Models for Semi-Solids

This study considers two models developed by Zavaliangos [29] and Burgos et al. [32]. Since semi-solid alloys with granular morphology exhibit low segregation under compression, particularly at low strains where localization tends to occur, the constitutive relations are formulated under undrained conditions, meaning deformation takes place at a constant total volume.

### 2.1. Zavaliangos constitutive model

Zavaliangos [29] modeled semi-solid deformation as an interpolation between two critical states: (i) porous material deformation, where grains are interconnected through cohesive bonds, and (ii) cohesionless granular deformation, where grain contacts are fully wetted by the liquid phase. The deformation behavior of semi-solid materials is described between these two extremes using a hyperelastic-viscoplastic framework. Under undrained conditions, the pressure of the liquid-phase is nearly equal to the hydrostatic stress within the solid skeleton, resulting in a stress state that is purely deviatoric. Therefore, only deviatoric stresses are considered, and the normality flow rule is expressed as:

$$\dot{\epsilon}_e = \sqrt{\frac{2}{3}} \dot{\epsilon}^p \cdot \dot{\epsilon}^p = \frac{\partial \mathcal{E}}{\partial \sigma_e} = \dot{\epsilon}_0 \left( \frac{\sigma_e}{\sigma_0} \right)^n A_c \frac{(n+1)}{2} \quad (1)$$

Where  $\dot{\epsilon}_e$  is the deviatoric part of the plastic strain

rate,  $\sigma_e$  is the von-Mises stress,  $\mathcal{E}$  is a viscoplastic potential,  $n$  is the power-law index,  $\dot{\epsilon}_0$  and  $\sigma_0$  are material parameters and  $A_c$  represents a function that accounts for the degree of cohesion and the liquid fraction:

$$A_c = \frac{1}{\left( \frac{1-c}{\sqrt{A_0}} + \frac{c}{\sqrt{A_1}} \right)^2} \quad (2)$$

Where  $c$  denotes the degree of cohesion, and  $A_0$  and  $A_1$  are also functions of the solid/liquid fraction, obtained through the following relations:

$$A_0 = \frac{4B_1}{\tan(\phi')^2} \quad (3)$$

$$B_1 = \frac{(3\alpha')^{\frac{2}{n+1}} (a_{contact})^{\frac{1}{n+1}}}{(1 - \beta' a_{contact})^2} \left( \frac{4\pi}{Z(1 - f_L) a_{contact}} \right)^{\frac{2n}{n+1}} \quad (4)$$

$$\alpha' = \frac{9\sqrt{\pi}}{4} \left( \frac{2n}{2n+1} \right)^{2(n-1)} \left( \frac{2n-1}{6n} \right)^n \quad (5)$$

$$\beta' = \frac{1}{\pi} \left( \frac{2n}{2n+1} \right)^{2(n-1)} \quad (6)$$

$$a_{contact} \approx 3(0.4 - f_L) \quad (7)$$

$$Z = 7.3 + 15.5 \left( 1 - \left( \frac{0.6}{1 - f_L} \right)^{0.33} \right) \quad (8)$$

$$A_1 = \frac{1}{(1 - f_L)^{10}} \quad (9)$$

Where  $\phi'$  represents the angle of the critical state line in the Cam-clay model and arises from the portion of solid grains with cohesionless contacts. Based on Eq. (2), the Zavaliangos constitutive relation under undrained condition can be finally expressed as:

$$\sigma_e = \sigma_0 \left( \frac{\dot{\epsilon}_e}{\dot{\epsilon}_0} \right)^m \left( \frac{1-c}{\sqrt{A_0}} + \frac{c}{\sqrt{A_1}} \right)^{(m+1)} \quad (10)$$

Where  $m = 1/n$  represents the rate sensitivity parameter. The hydrostatic pressure between grains or agglomerates may vary locally as a result of Reynolds dilatancy. To account for this, the internal friction arising

from grain sliding is also considered into the constitutive equation:

$$\sigma_e - \mu(\sigma_h - p_L) = \sigma_0 \left(\frac{\dot{\epsilon}_e}{\dot{\epsilon}_0}\right)^m \left(\frac{1-c}{\sqrt{A_0}} + \frac{c}{\sqrt{A_1}}\right)^{(m+1)} \quad (11)$$

Where  $\mu$  is the frictional coefficient, and  $\sigma_h - p_L$  represents the effective hydrostatic pressure, in accordance with Terzaghi's effective stress as defined in soil mechanics.

## 2.2. Burgos constitutive equation

Burgos et al. [32] proposed a constitutive model based on the Norton-Hoff law, in which the viscosity varies as a function of the cohesion degree ( $c$ ):

$$(\sigma_e)_{viscous} = 2\eta(c, \dot{\epsilon}_{eff})\dot{\epsilon}_{eff} \quad (12)$$

Where  $(\sigma_e)_{viscous}$  is the effective stress,  $\dot{\epsilon}_{eff}$  is the effective strain rate, and  $\eta(c, \dot{\epsilon}_{eff})$  is the viscosity expressed as a function of the cohesion degree and the effective strain rate:

$$\eta(c, \dot{\epsilon}_{eff}) = k(c)(\dot{\epsilon}_{eff})^{m(c)-1} \quad (13)$$

In the above equation,  $k(c)$  and  $m(c)$  are the functions of the cohesion degree:

$$k(c) = k_1 \exp(k_2 c) \quad (14)$$

$$m(c) = m_1 + m_2 c + m_3 c^2 \quad (15)$$

Where  $k_1, k_2, m_1, m_2$  and  $m_3$  are material constants. Considering the local variation of the effective hydrostatic pressure, Eq. (12) is finally written as:

$$(\sigma_e)_{viscous} - \mu(\sigma_h - p_L) = 2\eta(c, \dot{\epsilon}_{eff})\dot{\epsilon}_{eff} \quad (16)$$

## 3. Field Equilibrium Equations

### 3.1. Conservation of linear momentum

The principle of the conservation of linear momentum can be formulated as follows:

$$\text{div}\sigma + b = \rho\ddot{u} \quad (17)$$

Where  $b$  and  $u$  represent the internal forces and displacement, respectively. By neglecting the inertial

effects and internal forces, Eq. (17) is reduced to:

$$\text{div}\sigma = 0 \quad (18)$$

### 3.2. Conservation of mass

Assume  $M$  to be the amount of fluid crossing through a unit area per unit time, i.e., the fluid flux. According to Darcy's law,  $M$  is a function of the fluid pressure gradient:

$$M = -\chi\nabla p \quad (19)$$

Where  $\chi$  is the permeability. By introducing  $\zeta$  as the dilatational strain, the conservation of mass for the diffusion of fluid can be represented as:

$$\text{div}M + \dot{\zeta} = 0 \quad (20)$$

The normal (dilatational) strain rate,  $\dot{\zeta}$ , is obtained from the imposed shear strain rate via the following relation:

$$\dot{\zeta} = \beta\dot{\gamma} \quad (21)$$

Where  $\beta$  is the dilatancy ratio. Combining Eq. (19) with Eq. (20) results in:

$$\dot{\zeta} - \chi\nabla^2 p = 0 \quad (22)$$

In a supersaturated granular material, the rearrangement of grains is associated with the local dilatational strain, known as the Reynolds dilatancy.

## 4. Perturbation Analysis

For low solid fractions, the flow behavior of alloys in semi-solid state is typically investigated using a rheometer. In contrast, a hot compression test is commonly employed at high solid fractions, where the shearing state becomes more complex. For simplicity, we consider shearing deformation of an infinite layer with the normal in the y-direction, as shown in Fig. 1.

The plane strain condition is assumed, so the normal strain in the x direction is negligible. The properties of the layer are uniform in the x and z-directions, with a small perturbation introduced in the y direction. The balance law states that both shear and normal stresses

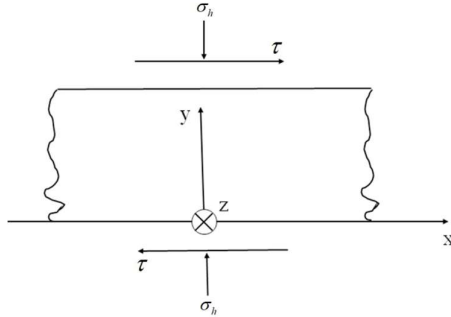


**Fig. 1.** An infinite layer subjected to shear under plane strain conditions, with the presence of compressive stress.

should remain homogeneous in the y-direction, i.e.,  $\tilde{\tau} = \tilde{\sigma}_h = 0$ . In the following, the condition for perturbation growth and subsequent localization is determined by considering each given constitutive model.

#### 4.1. Perturbation analysis based on Zavaliangos constitutive model

By considering  $B(c) = \left(\frac{1-c}{\sqrt{A_0}} + \frac{c}{\sqrt{A_1}}\right)$  in Zavaliangos model and taking the principle of momentum conservation into account, as described in Eq. (17) and (18), the perturbation in the linear form of Eq. (11) is as follows:

$$\frac{\mu \tilde{p}_L}{\sigma_e} = \tilde{m} \ln \dot{\varepsilon} + m \frac{\dot{\tilde{\varepsilon}}_e}{\dot{\varepsilon}_e} + \tilde{m} \ln B(c) + (1+m) \frac{B'(c)}{B(c)} \tilde{c} \quad (23)$$

Where  $B'(c)$  represents the derivation of  $B(c)$  with respect to the cohesion degree ( $c$ ). A quantity with tilde symbol denotes a small perturbation of the quantity. The growth or decay of this small perturbation over time determines the instability or stability of the system, respectively. Local dilatancy leads to a small decrease (perturbation) in the pressure of the liquid phase,  $\tilde{p}_L$ . The rate sensitivity parameter is considered constant in the Zavaliangos model, so  $\tilde{m} = 0$ . Therefore, Eq. (23) simplifies to:

$$\frac{\mu \tilde{p}_L}{\sigma_e} = m \frac{\dot{\tilde{\varepsilon}}_e}{\dot{\varepsilon}_e} + (1+m) \frac{B'(c)}{B(c)} \tilde{c} \quad (24)$$

Considering the perturbation of  $\varepsilon_e$  and  $c$  as  $\tilde{\varepsilon}_e = a^* \exp(i\xi x + \lambda t)$  and  $\tilde{c} = -a^* \exp(i\xi x + \lambda t)$ , respectively, where  $a^*$  is the wave amplitude referring to

the initial value at time  $t_0$  ( $a^* \ll 1$ ),  $\xi$  is the wave number in the y-direction normal to localized band, and  $\lambda$  is initial growth rate. Perturbation growth, and consequently instability, occurs when  $\lambda > 0$ , otherwise the deformation remains stable. The negative sign for  $\tilde{c}$  indicates that the perturbation in the cohesion degree is associated with its decrease. Therefore, Eq. (24) simplifies to:

$$\frac{\mu \tilde{p}_L}{\sigma_e} = \left[ m \frac{\lambda}{\dot{\varepsilon}_e} - (1+m) \frac{B'(c)}{B(c)} \right] a^* \exp(i\xi x + \lambda t) \quad (25)$$

The perturbation form of the mass conservation law, given by Eq. (22), can be written as:

$$\dot{\tilde{\zeta}} - \chi \nabla^2 \tilde{p}_L = 0 \quad (26)$$

Finally, by considering Eq. (21) for the dilatational strain rate, Eq. (26) can be rewritten for  $\lambda$  as:

$$\lambda = \frac{\dot{\varepsilon}_e (1+m) B'(c) \sigma_e \chi \xi^2}{B(c) [\mu \dot{\varepsilon}_e \beta + \sigma_e m \chi \xi^2]} \quad (27)$$

Since  $B'(c) > 0$ , the numerator has a positive value. The terms in denominator also have positive values. Consequently, it can be concluded that  $\lambda$  is positive for any perturbation. In other words, any perturbation leads to instability in the deformation. Indeed, Eq. (27) shows that  $\lambda(\xi)$  acts as a high-pass filter, meaning that modes with  $\xi \gg \sqrt{\frac{\mu \beta \dot{\varepsilon}_e}{\sigma_e m \chi}}$  grow at the maximum rate:

$$\lambda_{max} = \frac{\dot{\varepsilon}_e (1+m) B'(c)}{B(c) m} \quad (28)$$

Analogous to the interpretation of the necking phenomenon in tensile loading, failure can be categorized for instability. As stated in the aforementioned analysis, modes with high  $\xi$  grow at the maximum rate, indicating that localized failure is expected. Based on the definition of  $B(c)$ , the following relation is finally obtained:

$$\lambda_{max} = \dot{\varepsilon}_e \frac{(1+m)}{m} \left( \frac{1-c}{\sqrt{A_0}} + \frac{c}{\sqrt{A_1}} \right)^{-1} \left( \frac{1}{\sqrt{A_1}} - \frac{1}{\sqrt{A_0}} \right) \quad (29)$$

Eq. (29) reveals the retardant effect of the rate sensitivity on localization. It also demonstrates that the tendency of localization increases with the strain rate. However, it indicates that an increase in the cohesion degree, which is directly related to the solid fraction, can have a retarding effect on localization. This result contradicts recent experimental findings obtained via X-ray tomography. For example, [53] proposed a deformation mechanism for semi-solid materials analogous to that of geomaterials. The shear-induced dilation in such materials leads to have a critical state for solid fraction, beyond which pore opening and crack propagation occur during deformation. This contradiction arises from the assumption in Zavaliangos' mode that the ratio of porous material deformation to cohesionless granular deformation increases with increasing solid fraction. However, as recent findings suggest, the granular features of semi-solid deformation such as grain rearrangement, and agglomerates and Reynolds dilatancy, dominate at high solid fractions.

#### 4.2. Perturbation analysis based on Burgos constitutive model

Following a similar approach, linearizing the Burgos model results in:

$$\frac{\mu \tilde{p}_L}{\sigma_e} = \frac{k'(c)\tilde{c}}{k(c)} + m \frac{\dot{\gamma}}{\gamma} + m'(c)\tilde{c} \ln \dot{\gamma} \quad (30)$$

Where  $k'(c)$  and  $m'(c)$  are the derivatives of  $k(c)$  and  $m(c)$  with respect to  $c$ , respectively. Considering the perturbation of  $\tilde{\gamma}$  and  $c$  as  $\tilde{\gamma} = a^* \exp(i\xi x + \lambda t)$  and  $\tilde{c} = -a^* \exp(i\xi x + \lambda t)$ , Eq. (30) simplifies to:

$$\frac{\mu \tilde{p}_L}{\sigma_e} = \left[ -\frac{k'(c)}{k(c)} + m \frac{\lambda}{\gamma} - m'(c) \ln \dot{\gamma} \right] a^* \exp(i\xi x + \lambda t) \quad (31)$$

Based on Eq. (14), it obtains that  $\frac{k'(\psi)}{k(\psi)} = k_2$ . Hence, by considering the linear perturbation of the mass conservation relation, Eq. (22), it results in:

$$\lambda = \frac{\chi \frac{\sigma_e}{\mu} \xi^2 [k_2 + m'(c) \ln \dot{\gamma}] \dot{\gamma}}{\beta \dot{\gamma} + m \chi \frac{\tau}{\mu} \xi^2} \quad (32)$$

In Eq. (32), the denominator is always positive. Therefore, for the perturbation growth rate to be positive, the following condition must be satisfied:

$$k_2 + m'(c) \ln \dot{\gamma} > 0 \quad (33)$$

The sign of  $m'(c)$  can be determined by considering the following argument. If  $c = 0$ , the deformation is controlled by the liquid flow. Assuming the melt obeys Newtonian behavior, it can be concluded that  $m = 1$  for  $c = 0$ . On the other hand,  $c = 1$  represents the condition in which the deformation concentrates on solid bonds, so  $m$  can be considered as  $m_s$  (the rate sensitivity of viscoplastic deformation of solid bonds), which is much lower value than unity. This clearly shows that  $m(c)$  decreases with increasing  $c$ , so  $m'(c) < 0$ .

It is obvious that the resulting instability criterion depends on the material parameters. By taking  $m'(c) < 0$ , the instability condition simplifies to:

$$\ln \dot{\gamma} > \frac{k_2}{|m'(c)|} \quad (34)$$

The above relation indicates that for a given cohesion degree, there is a critical strain rate below which the deformation in the semi-solid state remains stable. This result is consistent with the observation that a decrease in strain rate reduces the ratio of peak to plateau stress, thereby lowering the tendency for shear localization. [17].

On the other hand, Eq. (32) shows that  $\lambda(\xi)$  acts as a high-pass filter, and modes with  $\xi \gg \sqrt{\frac{\mu \beta \dot{\epsilon}_e}{\sigma_e m \chi}}$ , similar to the results obtained from the Zavaliangos model, grow at the maximum rate:

$$\lambda_{max} = \frac{\dot{\gamma} [k_2 + m'(c) \ln \dot{\gamma}]}{m} \quad (35)$$

The above equation clearly reveals the retarding effect of rate sensitivity on shear localization. It also demonstrates that an increase in the strain rate enhances the tendency for shear localization. Furthermore, given that  $m'(c) < 0$ , the denominator decreases with increasing cohesion degree. This indicates that a higher cohesion degree increases the possibility of localization.

## 5. Experimental Verification

Compression test data for AA7075 aluminum alloy in the semi-solid state is used to validate the proposed analytical analysis.

The chemical composition of the AA7075 alloy is listed in Table 1.

The solid/liquid fraction versus temperature curve for AA7075 was obtained from the work of Binesh and Aghaie-Khafri [54], using the differential scanning calorimeter (DSC) method (Fig. 2).

Extruded AA7075 round bars (30 mm in diameter and 35 mm in height) initially compressed using a hydraulic press to achieve a 30% height reduction. Cylindrical specimens measuring 8 mm in diameter and 12 mm in height were then machined from the core of the compressed bars. These samples were subsequently heated to 585 °C, 600 °C, and 615 °C for 10 minutes and compressed at a strain rate of 0.3/s to examine deformation behavior at varying solid fractions. The corresponding solid fractions at 585 °C, 600 °C, and 615 °C were 0.93, 0.8, and 0.65, respectively.

**Table 1.** Chemical composition of wrought AA7075 aluminum alloy (wt.%)

| Al   | Mn   | Fe   | Cr   | Cu   | Mg   | Zn   | Si   |
|------|------|------|------|------|------|------|------|
| Bal. | 0.28 | 0.28 | 0.13 | 1.58 | 2.41 | 5.31 | 0.14 |

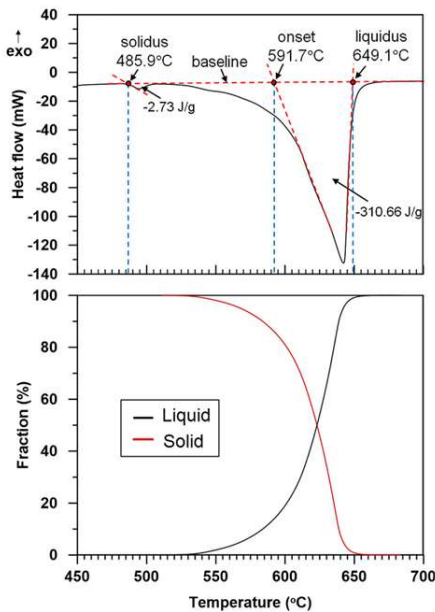


**Fig. 2.** (a) DSC curve of 7075 Al alloy at a heating rate of 10 °C/min, and (b) solid and liquid volume fraction versus temperature derived from the DSC curve [54].

The initial microstructures at these temperatures are presented in Fig. 3, where grain growth is clearly observed.

Since the cohesion degree represents the fraction of the solid skeleton formed within the semi-solid structure, its initial value can be estimated using the relationship proposed by Favier and Atkinson [39], which is based on the concept of percolation:

$$c = 1 - \frac{f_p}{f_s} \quad (36)$$

Where  $f_p$  is the percolation threshold represents the minimum solid fraction required to form a continuous skeleton capable of sustaining shear stress. Using a threshold value of 0.4, as reported in [39], the corresponding cohesion degrees were calculated and are presented in Table 2. The corresponding microstructures after compression are shown in Fig. 4.

The microstructures reveal that the specimens compressed at 585 °C and 600 °C exhibit deformation characterized by shear localization. In contrast, no damage bands are observed in the microstructure of the specimen compressed at 615 °C. This observation aligns well with the predictions of the Burgos model, which suggests that shear localization is suppressed as the cohesion degree decreases in semi-solid materials.

**Table 2.** Cohesion degrees at 585, 600, and 615 °C

| Temperature (°C) | Cohesion degree (c) |
|------------------|---------------------|
| 585              | 0.57                |
| 600              | 0.5                 |
| 615              | 0.38                |

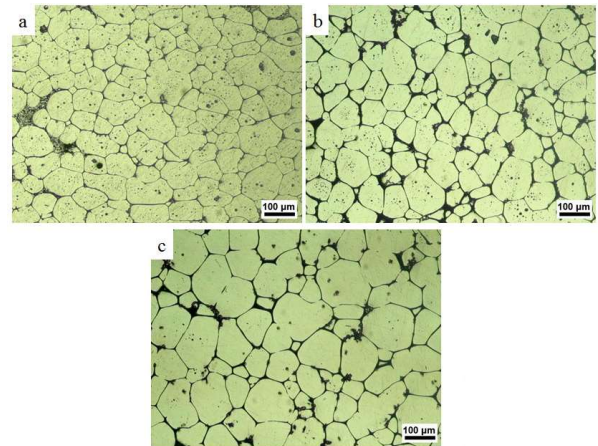


**Fig. 3.** The initial microstructures of AA7075 specimens compressed at (a) 585 °C, (b) 600 °C, and (c) 615 °C.

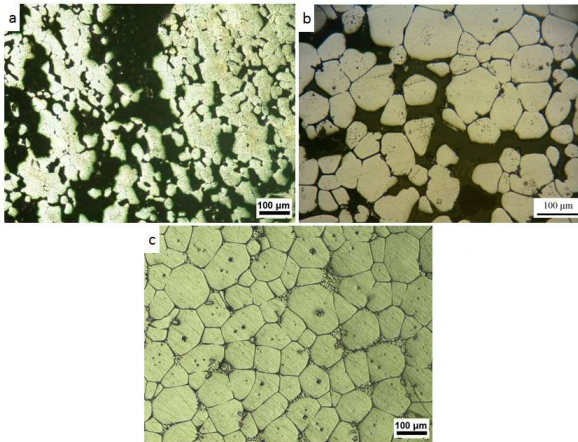


Fig. 4. Microstructures of the compressed specimens at (a) 585 °C, (b) 600 °C, and (c) 615 °C.

However, this finding contradicts the analysis based on the Zavaliangos model. To further investigate this discrepancy, Eq. (29) was parameterized by setting the rate sensitivity parameter to 0.2 and the critical state line angle  $\phi'$  to 28°, as reported in [17]. Using a Python script to implement Eqs. (3) through (9), the corresponding values of the maximum perturbation growth rate ( $\lambda_{max}$ ) were calculated and are presented in Table 3.

This suggests that increasing the cohesion degree reduces the maximum rate of perturbation growth and, consequently, lowers the likelihood of shear localization, an outcome that contradicts the available experimental evidence.

Table 3. Maximum rate of the perturbation growth at 585, 600 and 615 °C

| Temperature (°C) | $\lambda_{max}$ [1/s] |
|------------------|-----------------------|
| 585              | 0.59                  |
| 600              | 1.45                  |
| 615              | 1.81                  |

## 6. Conclusions

This study investigates the influence of constitutive modeling on shear localization during semi-solid deformation, comparing two distinct constitutive approaches: the Zavaliangos and Burgos models. The following key findings have emerged:

- For both models, the growth rate of perturbations  $\lambda(\xi)$  acts as a high-pass filter, meaning modes with  $\xi \gg \sqrt{\frac{\mu\beta\dot{\epsilon}_e}{\sigma_{em}\chi}}$  grow at maximum faster rate. This implies a tendency toward localized failure.

- Both models suggest that an increase strain rate promotes shear localization, while greater rate sensitivity has a stabilizing effect. The Zavaliangos model suggests that increasing cohesion degrees reduce localization tendency. However, this prediction contradicts experimental evidence, as confirmed by parameterization and comparison with microstructural observations.
- In contrast, the Burgos model demonstrates better agreement with experimental results, particularly those obtained via X-ray tomography, by indicating that higher cohesion enhances localization. The analysis also aligns well with the deformation behavior observed in compressed AA7075 specimens.
- Additionally, the Burgos model predicts the existence of a critical strain rate below which deformation remains stable, a result consistent with prior experimental findings.

Overall, these results underscore the critical role of constitutive model in accurately capturing the deformation mechanics of semi-solid materials. Selecting an appropriate model is essential for reliable prediction of localization behavior. Continued research, including more detailed experimental validation and model refinement, is necessary to further improve the accuracy and applicability of these constitutive frameworks.

## Conflict of interest

The authors declare that there is no conflict of interest.

## Funding

The authors declare that no funds, grants, or other support were received.

## 7. References

- [1] Flemings, M. C. (1991). Behavior of metal alloys in the semisolid state. *Metallurgical Transactions A*, 22(5), 957-981. <https://doi.org/10.1007/BF02661090>
- [2] Cho, W. G., & Kang, C. G. (2000). Mechanical properties and their microstructure evaluation in the thixoforming process of semi-solid aluminum alloys.

- Journal of Materials Processing Technology*, 105(3), 269-277.  
[https://doi.org/10.1016/S0924-0136\(00\)00656-6](https://doi.org/10.1016/S0924-0136(00)00656-6)
- [3] Kirkwood, D. H., Suéry, M., Kapranos, P., Atkinson, H. V., & Young, K. P. (2010). *Semi-solid processing of alloys* (Vol. 124). Berlin: Springer.  
<https://doi.org/10.1007/978-3-642-14355-0>
- [4] Nafisi, S., & Ghomashchi, R. (2016). *Semi-solid processing of aluminum alloys* (pp. 1-41). Cham, Switzerland: Springer International Publishing.  
[https://doi.org/10.1007/978-3-319-48159-4\\_1](https://doi.org/10.1007/978-3-319-48159-4_1)
- [5] Ji, S., Wang, K., & Dong, X. (2022). An overview on the process development and the formation of non-dendritic microstructure in semi-solid processing of metallic materials. *Crystals*, 12(8), 1044.  
<https://doi.org/10.3390/cryst12081044>
- [6] Ragheb, Z. D., Shabestari, S. G., & Najafi, Y. (2023). Effect of strain-induced melt activation process and thixoforming on microstructure and mechanical properties of 319 aluminum alloy. *Journal of Alloys and Compounds*, 954, 170152.  
<https://doi.org/10.1016/j.jallcom.2023.170152>
- [7] Li, S., Wang, Y., Li, Z., Liu, X., & Zhao, S. (2023). Study on the semi-solid thixotropic forging forming process for the low-carbon steel claw pole. *Materials*, 16(13), 4790.  
<https://doi.org/10.3390/ma16134790>
- [8] Huang, M., Jiang, J., Wang, Y., Liu, Y., Zhang, Y., & Dong, J. (2023). Thixotropic deformation behavior, rapid spheroidization and solid-liquid homogenization of semi-solid Al0.8Co0.5Cr1.5CuFeNi HEA with multilevel microstructure. *Scripta Materialia*, 229, 115384.  
<https://doi.org/10.1016/j.scriptamat.2023.115384>
- [9] Yuan, K., Lu, Y., Li, W., Yu, H., & Gao, S. (2022). Rheological characterization and accumulation tests for strong thixotropic engineering slurry. *Materials*, 15(19), 6891. <https://doi.org/10.3390/ma15196891>
- [10] Megalingam, A., Ahmad, A. H. B., Maarof, M. R. B., & Sudhakar, K. (2022). Viscosity measurements in semi-solid metal processing: current status and recent developments. *The International Journal of Advanced Manufacturing Technology*, 119(3), 1435-1459.  
<https://doi.org/10.1007/s00170-021-08238-4>
- [11] Keung, W. C., Lee, Y. F., Shan, W. W., & Luo, S. J. (2008). Thixotropic strength and thixotropic criteria in semi-solid processing. *Solid State Phenomena*, 141, 319-323.  
<https://doi.org/10.4028/www.scientific.net/SSP.141-143.319>
- [12] Petera, J., Kaminski, K., & Kotynia, M. (2010). A generalized viscoelastic Maxwell model for semisolid thixotropic alloys. *International Journal of Material Forming*, 3, 775-778. <https://doi.org/10.1007/s12289-010-0817-1>
- [13] Sheikh-Ansari, M. H., & Aghaie-Khafri, M. (2019). Constitutive modeling of semisolid deformation for the assessment of dilatant shear bands. *Applied Mathematical Modelling*, 70, 128-138.  
<https://doi.org/10.1016/j.apm.2019.01.019>
- [14] Sanjuan-Sanjuan, G., & Chavez-Castellanos, Á. E. (2019). Viscoelastic properties of thixotropic semisolid alloy relating the microstructure. *Solid State Phenomena*, 285, 380-384.  
<https://doi.org/10.4028/www.scientific.net/SSP.285.380>
- [15] Koke, J., & Modigell, M. (2003). Flow behaviour of semi-solid metal alloys. *Journal of Non-Newtonian Fluid Mechanics*, 112(2-3), 141-160.  
[https://doi.org/10.1016/S0377-0257\(03\)00120-9](https://doi.org/10.1016/S0377-0257(03)00120-9)
- [16] Modigell, M., Pola, A., & Tocci, M. (2018). Rheological characterization of semi-solid metals: a review. *Metals*, 8(4), 245. <https://doi.org/10.3390/met8040245>
- [17] Tzimas, E., & Zavaliangos, A. (1999). Mechanical behavior of alloys with equiaxed microstructure in the semisolid state at high solid content. *Acta Materialia*, 47(2), 517-528.  
[https://doi.org/10.1016/S1359-6454\(98\)00355-4](https://doi.org/10.1016/S1359-6454(98)00355-4)
- [18] Wang, K., Hu, S., Wang, T., Xie, W., Guo, T., Li, F., & Luo, R. (2022). Microstructural evolution and mechanical properties of 7075 aluminium alloy during semi-solid compression deformation. *Crystals*, 12(8), 1119. <https://doi.org/10.3390/cryst12081119>
- [19] Sheikh-Ansari, M. H., & Aghaie-Khafri, M. (2017). Assessment of Poliak-Jonas criterion for the onset of dynamic recrystallization in semi-solid deformation. *Materials Research Express*, 4(10), 106516.  
<https://doi.org/10.1088/2053-1591/aa9232>
- [20] Yamanaka, N., Sakane, S., & Takaki, T. (2021). Multi-phase-field lattice Boltzmann model for polycrystalline equiaxed solidification with motion. *Computational Materials Science*, 197, 110658.  
<https://doi.org/10.1016/j.commatsci.2021.110658>
- [21] Liu, X., Tang, F., Zhao, W., Cai, J., & Wei, Y. (2022). Multi-phase field lattice Boltzmann model of columnar-to-equiaxed transition in entire welding molten pool. *Computational Materials Science*, 204, 111182.  
<https://doi.org/10.1016/j.commatsci.2021.111182>
- [22] Su, T. C., Chen, M. C., Hu, H. R., Ko, Y. H., & Yao, L. E. (2023). Exploring semi-solid deformation of Al-Cu alloys by a quantitative comparison between drained die compression experiments and 3D discrete element method simulations. In *TMS Annual Meeting & Exhibition* (pp. 558-567). Cham: Springer Nature Switzerland.  
[https://doi.org/10.1007/978-3-031-22532-1\\_76](https://doi.org/10.1007/978-3-031-22532-1_76)

- [23] Karagadde, S., Lee, P. D., Cai, B., Fife, J. L., Azeem, M. A., Kareh, K. M., Puncreobutr, C., Tsvoulas, D., Connolly, T., & Atwood, R. C. (2015). Transgranular liquation cracking of grains in the semi-solid state. *Nature Communications*, 6(1), 8300. <https://doi.org/10.1038/ncomms9300>
- [24] Morita, S., Yasuda, H., Nagira, T., Gourlay, C. M., Yoshiya, M., & Sugiyama, A. (2012). Macroscopic modelling of semisolid deformation for considering segregation bands induced by shear deformation. In *IOP Conference Series: Materials Science and Engineering* (Vol. 33, No. 1, p. 012053). IOP Publishing. <https://doi.org/10.1088/1757-899X/33/1/012053>
- [25] Nagira, T., Morita, S., Yasuda, H., Gourlay, C. M., Yoshiya, M., Sugiyama, A., & Uesugi, K. (2015). Localization of shear strain and shear band formation induced by deformation in semi-solid Al-Cu alloys. In *IOP Conference Series: Materials Science and Engineering* (Vol. 84, No. 1, p. 012078). IOP Publishing. <https://doi.org/10.1088/1757-899X/84/1/012078>
- [26] Atkinson, H. V. (2005). Modelling the semisolid processing of metallic alloys. *Progress in Materials Science*, 50(3), 341-412. <https://doi.org/10.1016/j.pmatsci.2004.04.003>
- [27] Nguyen, T. G., Favier, D., & Suéry, M. (1994). Theoretical and experimental study of the isothermal mechanical behaviour of alloys in the semi-solid state. *International Journal of Plasticity*, 10(6), 663-693. [https://doi.org/10.1016/0749-6419\(94\)900280](https://doi.org/10.1016/0749-6419(94)900280)
- [28] Martin, C. L., Favier, D., & Suéry, M. (1997). Viscoplastic behaviour of porous metallic materials saturated with liquid part I: Constitutive equations. *International Journal of Plasticity*, 13(3), 215-235. [https://doi.org/10.1016/S0749-6419\(97\)00009-0](https://doi.org/10.1016/S0749-6419(97)00009-0)
- [29] Zavaliangos, A. (1998). Modeling of the mechanical behavior of semisolid metallic alloys at high volume fractions of solid. *International Journal of Mechanical Sciences*, 40(10), 1029-1041. [https://doi.org/10.1016/S0020-7403\(98\)00011-3](https://doi.org/10.1016/S0020-7403(98)00011-3)
- [30] Kang, C. G., & Jung, H. K. (1999). Finite element analysis with deformation behavior modeling of globular microstructure in forming process of semi-solid materials. *International Journal of Mechanical Sciences*, 41(12), 1423-1445. [https://doi.org/10.1016/S0020-7403\(98\)00107-6](https://doi.org/10.1016/S0020-7403(98)00107-6)
- [31] De Deus, H. P. A., Dupim, G. S. (2013). On behavior of the thixotropic fluids. *Physics Letters A*, 377(6), 478-485. <https://doi.org/10.1016/j.physleta.2012.12.011>
- [32] Burgos, G. (2001). Thixotropic rheology of semisolid metal suspension. *Journal of Materials Processing Technology*, 110, 53-58. [https://doi.org/10.1016/S0924-0136\(00\)00731-7](https://doi.org/10.1016/S0924-0136(00)00731-7)
- [33] Koeune, R., & Ponthot, J. P. (2014). A one phase thermomechanical model for the numerical simulation of semi-solid material behavior. Application to thixoforming. *International Journal of Plasticity*, 58, 120-153. <https://doi.org/10.1016/j.ijplas.2014.01.004>
- [34] Abali, B. E., Wu, C. C., & Müller, W. H. (2016). An energy-based method to determine material constants in nonlinear rheology with applications. *Continuum Mechanics and Thermodynamics*, 28, 1221-1246. <https://doi.org/10.1007/s00161-015-0472-z>
- [35] Chen, G., Lin, F., Yao, S., Han, F., Wei, B., & Zhang, Y. (2016). Constitutive behavior of aluminum alloy in a wide temperature range from warm to semi-solid regions. *Journal of Alloys and Compounds*, 674, 26-36. <https://doi.org/10.1016/j.matsciteng.2016.03.032>
- [36] Wang, J., Phillion, A. B., & Lu, G. (2014). Development of a visco-plastic constitutive modeling for thixoforming of AA6061 in semi-solid state. *Journal of Alloys and Compounds*, 609, 290-295. <https://doi.org/10.1016/j.jallcom.2014.04.140>
- [37] Cezard, P., Favier, V., Bigot, R., Balan, T., & Berveiller, M. (2005). Simulation of semi-solid thixoforging using a micro-macro constitutive equation. *Computational Materials Science*, 32(3-4), 323-328. <https://doi.org/10.1016/j.commatsci.2004.09.036>
- [38] Favier, V., Cezard, P., & Bigot, R. (2009). Transient and non-isothermal semi-solid behaviour: 3D micromechanical modelling. *Materials Science and Engineering: A*, 517(1-2), 8-16. <https://doi.org/10.1016/j.msea.2009.03.018>
- [39] Favier, V., & Atkinson, H. V. (2011). Micromechanical modelling of the elastic-viscoplastic response of metallic alloys under rapid compression in the semi-solid state. *Acta Materialia*, 59(3), 1271-1280. <https://doi.org/10.1016/j.actamat.2010.10.059>
- [40] Hill, R. (1962). Acceleration waves in solids. *Journal of the Mechanics and Physics of Solids*, 10(1), 1-16. [https://doi.org/10.1016/0022-5096\(62\)90024-8](https://doi.org/10.1016/0022-5096(62)90024-8)
- [41] Rudnicki, J. W., & Rice, J. R. (1975). Conditions for the localization of deformation in pressure-sensitive dilatant materials. *Journal of the Mechanics and Physics of Solids*, 23(6), 371-394. [https://doi.org/10.1016/0022-5096\(75\)90001-0](https://doi.org/10.1016/0022-5096(75)90001-0)
- [42] Young, N. J. B. (1976). Bifurcation phenomena in the plane compression test. *Journal of the Mechanics and Physics of Solids*, 24(1), 77-91. [https://doi.org/10.1016/0022-5096\(76\)90019-3](https://doi.org/10.1016/0022-5096(76)90019-3)
- [43] Nicot, F., Sibille, L., & Darve, F. (2012). Failure in rate-independent granular materials as a bifurcation toward a dynamic regime. *International Journal of Plasticity*, 29, 136-154. <https://doi.org/10.1016/j.ijplas.2011.08.002>
- [44] Śloderbach, Z. (2016). Closed set of the uniqueness conditions and bifurcation criteria in generalized coupled

- thermoplasticity for small deformations. *Continuum Mechanics and Thermodynamics*, 28, 633-654. <https://doi.org/10.1007/s00161-016-0924-4>
- [45] Baldelli, A. A. L., & Maurini, C. (2021). Numerical bifurcation and stability analysis of variational gradient-damage models for phase-field fracture. *Journal of the Mechanics and Physics of Solids*, 152, 104424. <https://doi.org/10.1016/j.jmps.2021.104424>
- [46] Lemonds, J., Needleman, A. (1986). Finite element analyses of shear localization in rate and temperature dependent solids. *Mechanics of Materials*, 5(4), 339-361. [https://doi.org/10.1016/0167-6636\(86\)90039-6](https://doi.org/10.1016/0167-6636(86)90039-6)
- [47] Anand, L., Kim, K. H., Shawki, T. G. (1987). Onset of shear localization in viscoplastic solids. *Journal of the Mechanics and Physics of Solids*, 35(4), 407-429. [https://doi.org/10.1016/0022-5096\(87\)90045-7](https://doi.org/10.1016/0022-5096(87)90045-7)
- [48] Batra, R. C., Chen, L. (2001). Effect of viscoplastic relations on the instability strain, shear band initiation strain, the strain corresponding to the minimum shear band spacing, and the band width in a thermoviscoplastic material. *International Journal of Plasticity*, 17(11), 1465-1489. [https://doi.org/10.1016/S0749-6419\(01\)00004-3](https://doi.org/10.1016/S0749-6419(01)00004-3)
- [49] Benallal, A., & Comi, C. (2003). Perturbation growth and localization in fluid-saturated inelastic porous media under quasi-static loadings. *Journal of the Mechanics and Physics of Solids*, 51(5), 851-899. <https://doi.org/10.1016/j.jems.2002.09.002>
- [50] Mayer, A. E., Borodin, E. N., & Mayer, P. N. (2013). Localization of plastic flow at high-rate simple shear. *International Journal of Plasticity*, 51, 188-199. <https://doi.org/10.1016/j.ijplas.2013.05.005>
- [51] Jacquy, A. B., Rattiez, H., & Veveakis, M. (2021). Strain localization regularization and patterns formation in rate-dependent plastic materials with multiphysics coupling. *Journal of the Mechanics and Physics of Solids*, 152, 104422. <https://doi.org/10.1016/j.jmps.2021.104422>
- [52] Garcke, H., Knopf, P., & Yayla, S. (2022). Long-time dynamics of the Cahn–Hilliard equation with kinetic rate dependent dynamic boundary conditions. *Nonlinear Analysis*, 215, 112619. <https://doi.org/10.1007/s00605-021-01334-y>
- [53] Kareh, K. M., Lee, P. D., Atwood, R. C., Connolley, T., & Gourlay, C. M. (2014). Revealing the micromechanisms behind semi-solid metal deformation with time-resolved X-ray tomography. *Nature Communications*, 5(1), 4464. <https://doi.org/10.1038/ncomms5464>
- [54] Bineh, B., & Aghaie-Khafri, M. (2016). RUE-based semi-solidprocessing: Microstructure evolution and effective parameters. *Materials & Design*, 95, 268-286. <https://doi.org/10.1016/j.matdes.2016.01.117>